PAPER

One-step bioprinting of endothelialized, self-supporting arterial and venous networks

IOP Publishing Biofabrication 17 (2025) 025012 https://doi.org/10.1088/1758-5090/adab26

Biofabrication

PAPER

One-step bioprinting of endothelialized, self-supporting arterial and venous networks

RECEIVED
24 September 2024

REVISED
11 December 2024

ACCEPTED FOR PUBLICATION
16 January 2025

PUBLISHED
11 February 2025

Betty Cai[1], David Kilian[1], Sadegh Ghorbani[1,2], Julien G Roth[3], Alexis J Seymour[4], Lucia G Brunel[5], Daniel Ramos Mejia[1], Ricardo J Rios[1], Isabella M Szabo[1], Sean Chryz Iranzo[1], Andy Perez[1], Rameshwar R Rao[6,7], Sungchul Shin[8,*] and Sarah C Heilshorn[1,*]

[1] Department of Materials Science and Engineering, Stanford University, Stanford, CA 94305, United States of America
[2] Department of Health Technology, Technical University of Denmark, Kongens Lyngby 2800, Denmark
[3] Institute for Stem Cell Biology and Regenerative Medicine, Stanford University, Stanford, CA 94305, United States of America
[4] Department of Bioengineering, Stanford University, Stanford, CA 94305, United States of America
[5] Department of Chemical Engineering, Stanford University, Stanford, CA 94305, United States of America
[6] Ben Towne Center for Childhood Cancer and Blood Disorders Research, Seattle Children's Research Institute, Seattle, WA 98101, United States of America
[7] Division of Pediatric Hematology, Oncology, Bone Marrow Transplant, and Cellular Therapies, Department of Pediatrics, University of Washington School of Medicine, Seattle, WA 98105, United States of America
[8] Department of Agriculture, Forestry, and Bioresources, Seoul National University, Seoul 08826, Republic of Korea
* Authors to whom any correspondence should be addressed.

E-mail: sungssc@snu.ac.kr and heilshorn@stanford.edu

Keywords: 3D bioprinting, endothelialization, vascular mimics, arterial–venous networks

Supplementary material for this article is available online

Abstract

Advances in biofabrication have enabled the generation of freeform perfusable networks mimicking vasculature. However, key challenges remain in the effective endothelialization of these complex, vascular-like networks, including cell uniformity, seeding efficiency, and the ability to pattern multiple cell types. To overcome these challenges, we present an integrated fabrication and endothelialization strategy to directly generate branched, endothelial cell-lined networks using a diffusion-based, embedded 3D bioprinting process. In this strategy, a gelatin microparticle sacrificial ink delivering both cells and crosslinkers is extruded into a crosslinkable gel precursor support bath. A self-supporting, perfusable structure is formed by diffusion-induced crosslinking, after which the sacrificial ink is melted to allow cell release and adhesion to the printed lumen. This approach produces a uniform cell lining throughout networks with complex branching geometries, which are challenging to uniformly and efficiently endothelialize using conventional perfusion-based approaches. Furthermore, the biofabrication process enables high cell viability (>90%) and the formation of a confluent endothelial layer providing vascular-mimetic barrier function and shear stress response. Leveraging this strategy, we demonstrate for the first time the patterning of multiple endothelial cell types, including arterial and venous cells, within a single arterial–venous-like network. Altogether, this strategy enables the fabrication of multi-cellular engineered vasculature with enhanced geometric complexity and phenotypic heterogeneity.

1. Introduction

The fabrication of complex engineered vasculature is vital for a variety of applications, from *in vitro* models for drug screening and disease modeling to implantable devices for tissue repair [1–3]. Native vasculature is a complex, branched structure that includes vessels of multiple sizes connected together to form both arteries and veins [4–6]. While several advanced biofabrication approaches have been developed to fabricate vascular mimics [7–12], key challenges remain in creating perfusable, cell-lined structures that replicate both the geometric complexity and biological heterogeneity of arterial and venous networks. In particular, the endothelialization of engineered networks is crucial to the formation of the endothelial cell lining that underlies vascular function *in vivo* [5, 6]. While advancements in biofabrication

have enabled the generation of increasingly complex, 3D branched structures [8–11, 13, 14], the endothelialization of these vascular-like networks is especially challenging, particularly for structures that include multiple channel diameters within a single network. The predominant method for endothelialization involves perfusing the structure with an endothelial cell suspension [11–16], which can be a time-consuming processing step and often results in an inhomogeneous cell distribution despite extensive iterative optimization [17]. To overcome this challenge, *in situ* endothelialization approaches have been developed, where endothelial cells are incorporated into the printed structure during the bioprinting process [17–22]. To date, however, this promising strategy of *in situ* endothelialization has not been demonstrated with biofabrication techniques that generate cell-lined networks with multiple branches, varying channel diameters, and multiple endothelial cell types. Towards the broader biofabrication goal of creating more realistic engineered vasculature, here we developed an *in situ* endothelialization process that allows for the one-step fabrication and venous/arterial endothelialization of branched, self-supporting networks.

Due to its ability to rapidly generate customizable, perfusable structures, 3D bioprinting has emerged as a promising approach to fabricate complex engineered vasculature [5, 23]. Various 3D bioprinting methods have been employed for fabricating vascular mimics, the most common of which include layer-by-layer, coaxial, and sacrificial ink extrusion printing. In layer-by-layer printing, a hollow structure is fabricated by directly depositing filaments to form the channel walls [24–26], while in coaxial extrusion, a core–shell nozzle is used to extrude a filament with a hollow lumen [9, 21, 27–31]. As an alternative approach, the extrusion printing of a sacrificial ink has been used to pattern hollow networks within a gel precursor matrix [11–13, 32, 33]. Compared to other bioprinting modalities, this method is especially well suited to patterning perfusable networks with tunable diameters and freeform branching geometries. However, sacrificial ink extrusion has conventionally been used to pattern hollow networks within a bulk hydrogel instead of self-supporting, perfusable structures [11–13, 32, 33]. To fabricate self-supporting vascular-like networks, an emerging bioprinting method combines sacrificial ink extrusion with diffusion-based gelation [33–35]. In one example, termed gelation of uniform interfacial diffusant in embedded 3D printing (GUIDE-3DP), self-supporting channels are fabricated by including a crosslink initiator within the sacrificial ink [33]. After printing, the crosslink initiator diffuses from the sacrificial ink into the surrounding gel precursor matrix, allowing a shell of material surrounding the ink filament to be crosslinked. Using this diffusion-based 3D printing strategy, self-supporting, perfusable networks can be fabricated from a library of different biomaterials, with precise control over the branching geometry and vessel diameters [33].

Despite significant advances, all of these strategies typically require a post-fabrication step to introduce endothelial cells into the lumen through perfusion of a cell suspension [11, 12, 32, 33, 35]. Perfusion-based seeding is inefficient and often results in a non-uniform cell distribution in complex networks [17]. This limitation is especially pronounced in networks of channels with differing diameters due to unbalanced perfusion flow rates [10, 36, 37]. To overcome this challenge, we develop and optimize an *in situ* endothelialization approach where endothelial cells are included within the sacrificial ink during GUIDE-3DP fabrication. In addition to allowing the bioprinting of freeform, branched networks, this approach enables the patterning of multiple endothelial cell populations within a bioprinted network. This is especially important for the future fabrication of more biomimetic vascular models, since structures containing only a single endothelial cell population do not replicate the cellular diversity of *in vivo* vasculature. While bioprinting strategies thus far have only incorporated one endothelial cell type, the human vasculature is composed of diverse endothelial cell subsets that vary along the vascular tree as well as between organs (e.g. heart, brain, lung, and liver) and vascular systems (e.g. arterial, venous, capillary, and lymphatic) [38, 39]. Within the vascular network, different cell populations exhibit distinct characteristics, such as morphology, proliferation, inflammatory response, and barrier function, to fulfill specialized biological roles [40]. In the future, multi-cellular vascular models will be necessary to investigate the distinct cellular behaviors of different endothelial cell populations, as well as their signaling interactions which are crucial to understanding cell segregation and specification in vascular development [41]. Towards that larger goal, new biofabrication approaches are necessary to fabricate complex vascular constructs with the efficient patterning of multiple endothelial cell types.

To enable the fabrication of complex networks with multiple endothelial cell populations, we propose a biofabrication approach that integrates diffusion-induced print generation with *in situ* sacrificial ink-based endothelialization. In this strategy, complex, self-supporting networks are generated and uniformly endothelialized using the sacrificial ink as the carrier for both cells and crosslinkers. Importantly, our approach has the ability to incorporate multiple endothelial cell populations, including both arterial and venous endothelial cells, into a branched network with varying vessel diameters. Altogether, this work represents an important advance towards the fabrication of more biomimetic

vascular models replicating both the structural complexity and cellular heterogeneity of vasculature.

2. Results

2.1. Design of one-step fabrication and endothelialization approach for self-supporting, perfusable structures

For the integrated fabrication and endothelialization of self-supporting, perfusable structures, we designed a strategy based on freeform extrusion printing of a cell-delivering sacrificial ink into a gel precursor support material (figures 1(A) and (B)). In this strategy, first, the geometry of the internal lumen structure is printed using a sacrificial ink that includes a diffusible crosslink initiator. After sacrificial ink printing, the crosslink initiator is allowed to diffuse from the ink filament into the surrounding gel precursor support bath (figure 1(A), step 1). Following crosslink initiator diffusion, the crosslinking reaction is initiated, thus crosslinking the shell of material that contains both the gel precursor and the crosslink initiator (figure 1(A), step 2). The uncrosslinked gel precursor can then be removed to yield a self-supporting structure. To endothelialize the printed structure in the same fabrication step, we employed a slurry of gelatin microparticles as the sacrificial ink which, at the same time, serves as a cell-delivering bioink from which cells are released during melting at 37 °C (figure 1(A), step 3). After cells have been allowed to adhere to all sides of the printed lumen, the melted sacrificial ink is removed by cutting the print ends, resulting in a hollow, cell-lined structure (figure 1(A), step 4). We demonstrated this approach using a gelatin methacryloyl (GelMA)-based support material, which is photocrosslinked using a photoinitiator (lithium phenyl-2,4,6-trimethylbenzoylphosphinate, LAP) loaded in the sacrificial ink. For the support material, we employed a formulation consisting of GelMA (20 wt%), fibrinogen (0.5 wt%), and a viscosity modifier Aristoflex Ammonium Acryloyldimethyltaurate/VC Copolymer (AVC; 2 wt%). The addition of the viscosity modifier provides the support material with suitable rheological properties for embedded 3D bioprinting (figure S1), while the addition of fibrinogen enhances cellular adhesion *in vitro* [42]. Using this material, self-supporting, perfusable structures with high structural integrity can be fabricated (figure S2). The channel inner diameter can be controlled by varying the extrusion flow rate (table S1). To tune the outer diameter of printed channels, the wall thickness can be modulated by varying the crosslink initiator concentration and diffusion time (figure S3).

As a key advantage compared to perfusion-based seeding with a cell suspension, our strategy overcomes the common challenge associated with achieving a uniform cell distribution in complex networks [17, 43]. In a printed network where channels are intricately connected both in parallel and in series configurations, the pressure drop—and hence fluid flow rate—will depend on the internal diameter, channel segment length, and channel segment position within the overall network. This leads to variations in the flow rates within each channel. For a representative printed network (figure 1(C)), flow rates were predicted using finite element modeling (figure 1(D), panel i; video S1). This revealed significantly lower flows in vessels with smaller diameters, which was confirmed using fluorescent tracer particles (figure 1(D), panel ii). Thus, perfusion-based seeding of an endothelial cell suspension through a complex network such as this results in nonuniform cell delivery due to the uneven flow rates. In contrast, our sacrificial ink-based method directly deposits endothelial cells throughout the entire printed structure, resulting in uniform endothelialization of networks with freeform branching geometries (figure 1(E)).

By depositing cells onto the printed lumen *in situ*, our sacrificial ink-based seeding approach enables a more uniform cell distribution than conventional perfusion-based seeding. While the homogeneity of perfusion seeding is dependent on uniform fluid flow, the flow rates within a complex, branched network can vary greatly depending on the size and orientation of individual branches [36, 37]. To quantitatively compare perfusion- and sacrificial ink-based seeding, we designed three network structures that represent commonly encountered geometric variations. First, we demonstrated a structure with two branches of different inner diameters ($d_1 = 2d_2$), where the perfused fluid will exhibit a lower velocity through the channel with a smaller cross-sectional area. As a result, upon complete fluid perfusion through the thicker channel, the thinner channel will not yet be completely perfused (figure 2(A), panel i). The difference in flow rate and resulting particle distribution was validated using a finite element model of particle flow through the asymmetrical structure (figure 2(A), panel ii; video S2). For the perfusion-based seeding of structures with endothelial cells, a cell suspension was injected until the cells reached the outlet of the structures. After incubating for 10 min for cell adhesion onto the channel lumen, the number of attached cells was counted. In the case of perfusion seeding, almost no cells were observed in the channel with a smaller inner diameter (figure 2(A), panel iii). In contrast, when sacrificial ink seeding was used, cells were observed throughout the network, regardless of location, after sacrificial ink removal (figure 2(A), panel iv). As expected, fewer cells were observed in the branch with a smaller diameter because a smaller amount of bioink is extruded to form these smaller channels (figure 2(A), panel iv; figure S4). As a second test print, we demonstrated that a structure with branches positioned at different angles to the inlet ($\theta_1 = 0°$, $\theta_2 = 45°$) will also result in

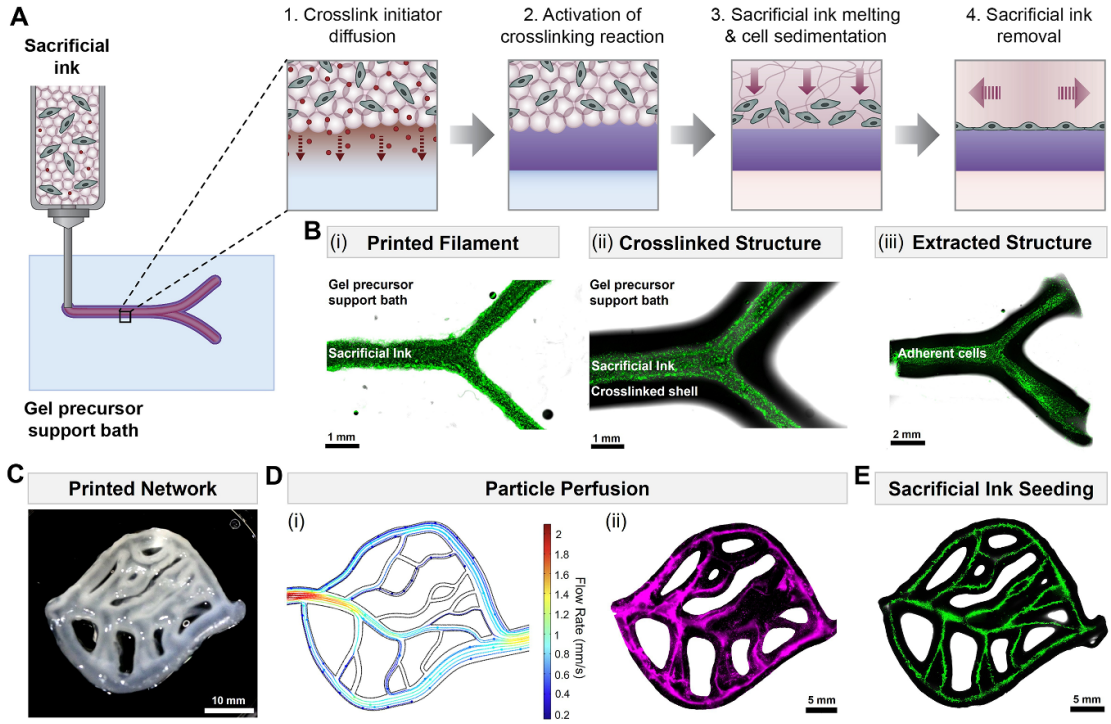

Figure 1. Fabrication and sacrificial ink-based endothelialization of self-supporting, perfusable structures. (A) Key steps of sacrificial ink-based endothelialization process, shown by a series of insets representing the ink-bath interface over time: (1) A sacrificial bioink (pink spheres) containing cells and a crosslink initiator (red dots) is extruded into a crosslinkable gel precursor support bath (light blue). The crosslink initiator diffuses across the ink interface into the surrounding gel precursor. (2) The crosslinking reaction is activated in a shell of material (purple) surrounding the printed sacrificial ink filament. (3) The printed structure is removed from the support bath, and then the sacrificial ink is melted, allowing the cells to sediment and adhere onto the print lumen. The structure is flipped to endothelialize the entire lumen surface. (4) The closed ends of the printed construct are cut open to create a perfusable network, allowing removal of the liquified sacrificial ink. (B) Composite images (brightfield and fluorescence to detect fluorophore-labeled endothelial cells) of (i) the printed, cell-containing sacrificial ink filament in the support bath before crosslinking, (ii) the crosslinked shell surrounding the printed sacrificial ink filament, and (iii) the final structure after removal of the support bath and sacrificial ink, leaving behind an endothelialized lumen. (C) Image of printed vascular-like network with interconnected branches. (D) Perfusion results in non-uniform distributions for complex structures due to heterogeneous flow rates, as shown by (i) a finite element model of particle flow and (ii) composite image of perfusion with a suspension of fluorescent particles (magenta). (E) Sacrificial ink seeding enables the uniform deposition of endothelial cells throughout all branches of a complex, interconnected network (human umbilical vein endothelial cells labeled in green with CellTracker).

non-homogeneous fluid flow (figure 2(B), panels i–ii; video S3). With perfusion seeding, a non-uniform distribution of cells was observed, with fewer cells present in the angled branch as compared to the straight branch (figure 2(B), panel iii). In contrast, the sacrificial ink seeding method ensures a homogeneous distribution of cells throughout the printed structure (figure 2(B), panel iv). As a third demonstration, we showed that two branches of varying length ($L_2 = 3L_1$) also result in non-uniform deposition of perfused cells, with the longer branch being inhomogeneously seeded (figure 2(C), panels i–iii; video S4). In contrast, sacrificial ink seeding results in an uniform cell distribution throughout both branches (figure 2(C), panel iv).

In addition to a more uniform cell distribution, sacrificial ink seeding has the inherent advantage of allowing a greater cell seeding efficiency. Perfusion seeding requires a greater number of cells to completely seed an asymmetrically branched structure due to differences in the rate at which individual branches are perfused. Cell loss is incurred as cells flow out of the fully perfused segments while the remaining segments are still being filled. With increasing complexity of the printed network, the seeding efficiency decreases as the differences in segment length and flow velocity become more pronounced. Although the representative structures shown in figure 2 may be more uniformly endothelialized by extending the perfusion time, the seeding efficiency would continually decrease during the additional perfusion period (figure S5). For example, during the additional time required to fully perfuse the longer channel shown in figure 2(C), cells will continuously flow out of the structure through the shorter channel, thus reducing the cell seeding efficiency. For this representative structure, the theoretical seeding efficiency for complete, uniform perfusion was estimated to be 30.7% using a finite element model of particle flow (figure S5(C), panel iii), where the number of particles retained in the lumen was divided by the total number of particles that entered the structure. In contrast to the inherent cell leakage present in perfusion seeding, the theoretical maximal

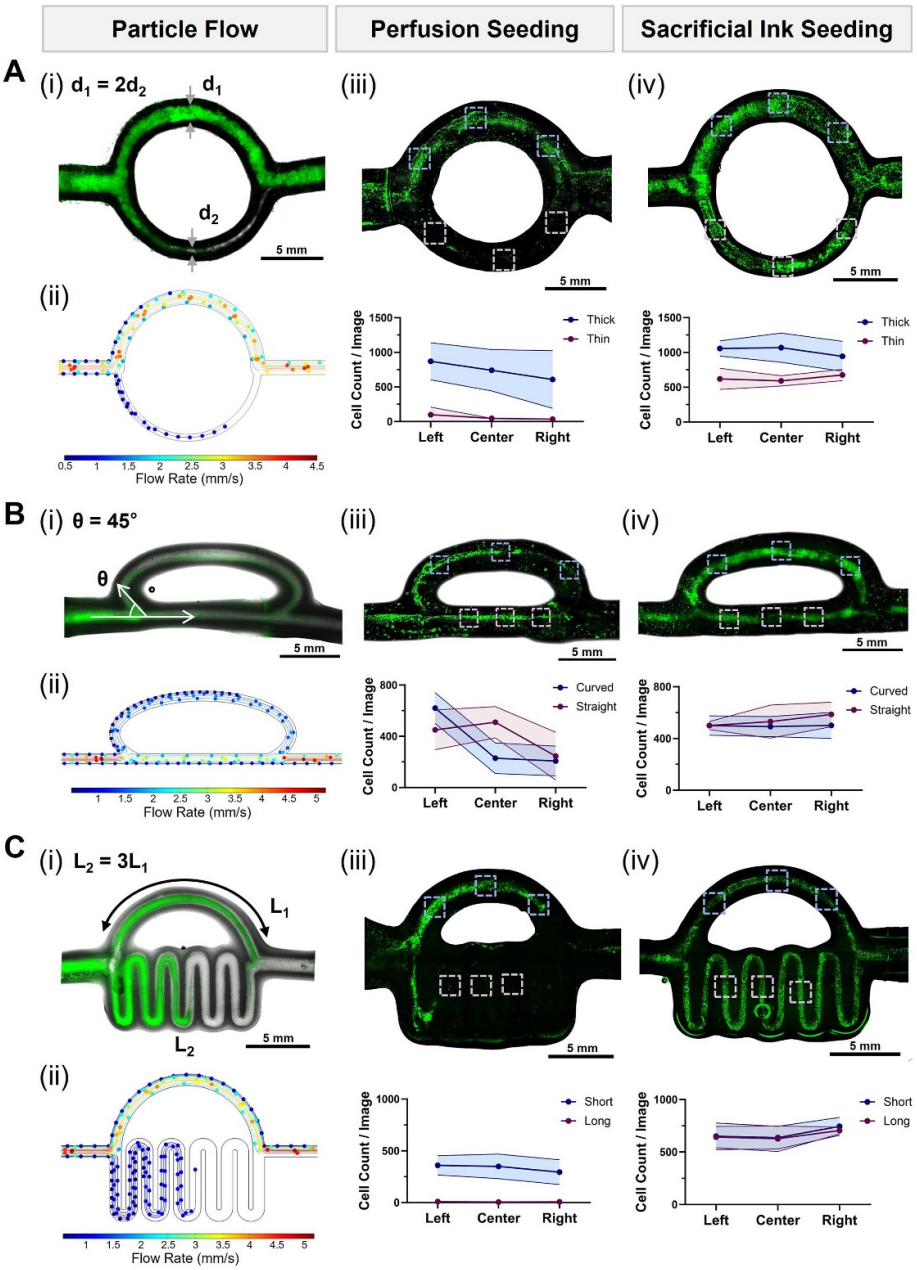

Figure 2. Sacrificial ink seeding provides a more uniform cell distribution than perfusion seeding. For representative geometries with branches of varying (A) diameters ($d_1 = 1.7 \pm 0.1$ mm, $d_2 = 0.9 \pm 0.1$ mm), (B) angles ($\theta = 45 \pm 1°$), and (C) lengths ($L_1 = 16.9 \pm 1.1$ mm, $L_2 = 50.5 \pm 0.5$ mm): (i) image of printed structure during fluorescent particle perfusion, (ii) representative finite element model indicating particle flow trajectories, (iii) image of printed structure after perfusion seeding with human umbilical vein endothelial cells (HUVEC) and associated cell counts in marked regions, and (iv) image of printed structure after sacrificial ink-based endothelialization and associated cell counts in marked regions. Cell count data points are averages and the shaded bands represent the standard deviations from $n = 3$ different printed structures for each geometry.

seeding efficiency for sacrificial ink-based seeding would be 100% when the same metric as perfusion seeding is applied. This is because cells are confined within the print lumen during the entire sacrificial ink seeding process. Since the crosslink initiator diffuses radially from the ink filament, a shell of gel precursor material surrounding the printed filament is crosslinked, resulting in a completely closed structure with no inherent cell loss. After the endothelialization process, the ends of the closed structure are cut open to create a perfusable network and allow sacrificial ink removal.

Here, we demonstrate the generation of self-supporting, endothelialized structures by combining sacrificial ink-based endothelialization with diffusion-based vessel generation. This integrated strategy is especially advantageous since self-supporting structures are challenging to endothelialize by perfusion. For non-embedded, self-supporting structures, perfusion seeding requires either connection to a pump setup or manual injection of a cell suspension [13, 30, 33]. Both strategies are expected to be challenging for small-diameter vessels (e.g. <1 mm diameter) and complex structures with

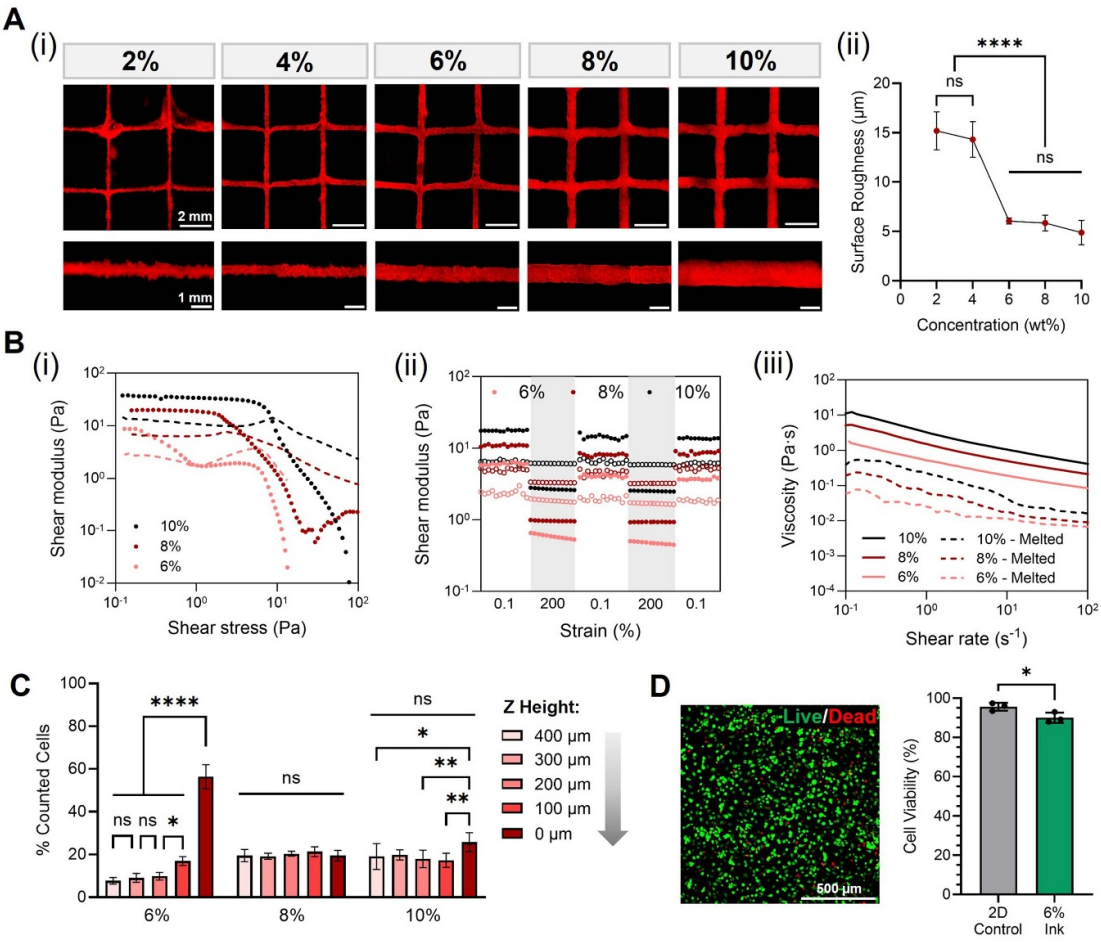

Figure 3. The gelatin microparticle sacrificial ink is optimized for printability and ability to support endothelial cell sedimentation. (A) The fidelity of the printed filament depends on gelatin microparticle concentration (2–10 wt%), as shown by (i) fluorescence images as well as (ii) the corresponding filament surface roughness ($n = 4$–5, ordinary one-way ANOVA with Tukey's multiple comparisons test, ns: not significant, $^{****}p < 0.0001$). (B) In shear rheology, gelatin microparticle inks with concentrations of 6–10 wt% exhibit (i) a yield stress, (ii) self-healing behavior (G', filled symbols; G", hollow symbols), and (iii) shear-thinning and thermo-responsive viscosity. (C) Cells encapsulated in the 6 wt% gelatin microparticle ink exhibit significantly greater cell sedimentation after 30 min as compared to 8 and 10 wt% inks ($n = 6$, two-way repeated measures ANOVA with Šídák's multiple comparisons test, ns: not significant, $^{*}p < 0.05$, $^{**}p < 0.01$, $^{****}p < 0.0001$). (D) Cells released from the 6 wt% gelatin microparticle ink exhibit high viability after 1 d of culture ($n = 3$, unpaired t test, $^{*}p < 0.05$).

variable vessel dimensions. As the above results indicate, sacrificial ink-based endothelialization allows for uniformly seeded, self-supporting vessels of varying diameters and branching geometries without extensive manipulation. Our integrated strategy therefore provides greater reproducibility and scalability than perfusion-based seeding after vessel fabrication.

2.2. Modular design of sacrificial ink with optimal printability and ability to support cell sedimentation

In our proposed strategy, the sacrificial ink is designed to fulfill three functions: first, the deposition of the sacrificial ink specifies the geometry of the internal lumen; second, the sacrificial ink serves as a reservoir for crosslink initiators that radially diffuse into the gel precursor support bath to form self-supporting channel walls; and third, the sacrificial ink delivers endothelial cells to the vessel lumens throughout the printed construct. To design a sacrificial ink that enables these functions, we selected gelatin microparticles as a cytocompatible material that can be readily removed by melting. To identify the concentration of gelatin microparticles for the sacrificial ink, we first evaluated the print resolution for five different formulations spanning 2–10 wt%. Inks with concentrations of 6–10 wt% produced smooth filaments with good shape fidelity and seamless junction points after printing into a support bath of GelMA (20 wt%) blended with AVC (2 wt%) (figure 3(A)). Rheological analysis confirmed that these inks possessed suitable rheological properties for extrusion, including yield-stress, self-healing, and shear-thinning behaviors (figure 3(B)).

In addition to providing high printability, the sacrificial ink must possess a sufficiently low viscosity after melting to enable rapid cell sedimentation. The viscosity of the melted ink was found to increase with increasing gelatin microparticle concentration, with 8 and 10 wt% inks having approximately two-

Table 1. Effect of gelatin microparticle concentration (6–10 wt%) on ink zero-shear viscosity; theoretical average Brownian displacement (x) of a neutrally buoyant, 15 μm sphere over 30 min; and theoretical sedimentation velocity (v) of a 15 μm sphere of density 1.03 g cm^{-3}.

	Unmelted ink			Melted ink		
Gelatin microgel conc. (wt%)	Zero-shear viscosity (Pa·s)	x (μm)	v (μm s^{-1})	Zero-shear viscosity (Pa·s)	x (μm)	v (μm s^{-1})
6	1.83 ± 0.87	0.24	0.008	0.079 ± 0.029	1.17	0.186
8	5.14 ± 0.66	0.14	0.003	0.196 ± 0.094	0.75	0.075
10	11.1 ± 3.7	0.10	0.001	0.383 ± 0.099	0.53	0.038

and five-fold higher viscosities than the 6 wt% ink, respectively (figure 3(B), table 1). Due to this difference in viscosity, the theoretical average displacement of cells due to Brownian motion, as well as the theoretical cell sedimentation velocity, will decrease with increasing gelatin microparticle concentration (table 1). To experimentally quantify cell sedimentation within both melted and unmelted inks, cells encapsulated within 6–10 wt% inks were incubated at either room temperature or 37 °C and imaged by fluorescence time-lapse microscopy across a height of 400 μm. Over 30 min, no cell sedimentation was observed in all unmelted gelatin microparticle inks (figure S6). In contrast, significant cell sedimentation was observed in the 6 wt% melted ink, while less sedimentation (i.e. more homogeneous cell distributions) was observed in the 8 and 10 wt% inks after 30 min of incubation at 37 °C (figure 3(C)). The observed sedimentation within the 6 wt% melted ink over a depth of 400 μm corresponds well with the theoretically predicted sedimentation distance of ∼335 μm (i.e. 0.186 μm s^{-1} over 30 min). Based on these results, we hypothesized that the 6 wt% gelatin microparticle ink would enable cells to sediment and adhere onto an underlying substrate within ∼15–30 min for channels of radius ∼150–500 μm. To assess cell viability after release from the ink, we incubated the cell-laden ink at 37 °C for 15 min to allow ink melting and cell sedimentation onto a culture substrate. After this incubation step, cells were cultured with the addition of 10x ink volume of fresh cell culture medium. Cells released from the 6 wt% gelatin microparticle ink exhibited high viability (88 ± 4%) at 1 d post-seeding, which was slightly lower than that for cells seeded directly from suspension (96 ± 2%; figure 3(D)). Altogether, these results encouraged us to further explore the endothelial cell phenotype after release from the 6 wt% gelatin microparticle ink within printed, perfusable channels.

2.3. Evaluation of endothelial cell viability, proliferation, and function within sacrificial ink-seeded structures

To provide vascular-mimetic biofunctionality, the printed structure must support endothelial cell attachment, viability, and proliferation. Using a Live/Dead cytotoxicity assay, we first demonstrated that sacrificial ink-seeded HUVEC maintained high viability in bioprinted GelMA (20 wt%) + fibrinogen (0.5 wt%) + AVC (2 wt%) channels (93 ± 4% on day 1, 93 ± 3% on day 7, $n = 4$ channels; figure 4(A)). Upon release from the sacrificial ink, cells were able to readily attach to the luminal surface of printed channels (figure S7(A)).

Additionally, the sacrificial ink-based endothelialization process enabled homogeneous cell seeding across the channel perimeter. After incubation for 10 min on both the top and bottom surfaces, a uniform cell density was observed on both halves of seeded channels (figure S7(B)). A 3D reconstruction of the cell-lined channel further confirmed that viable HUVEC populated the entire channel perimeter (figure 4(B)). A stable endothelial monolayer was formed within 5 d of culture, as indicated by immunostaining for F-actin, von Willebrand factor (vWF), and the adherens junction marker VE-cadherin (figure 4(C), panel i). Moreover, a confluent monolayer of endothelial cells was maintained over 14 d of culture, with cell–cell junctions marked by the expression of VE-cadherin (figure 4(C), panel ii). Actin filaments were observed to terminate at VE-cadherin-based junctions, indicating the linkage of actin to VE-cadherin, which is known to be essential for the stabilization of endothelial cell–cell contacts [44, 45]. As a control, channels seeded by perfusion with a HUVEC suspension after printing also demonstrated high cell viability and the formation of an endothelial monolayer (figure S8).

The morphological evidence of cell–cell junctions encouraged us to evaluate their functional activity, since a key function of the vascular endothelium is to form a semipermeable barrier controlling the transport of fluids and solutes [46]. To evaluate the permeability of the endothelial lining, a solution of 70 kDa rhodamine-dextran was injected into lumens with and without seeded HUVEC. Dye diffusion was assessed using time-lapse fluorescence microscopy (figure 4(D), panels i–ii). The diffusion of dextran into the channel walls after 0 and 30 min was quantified based on the fluorescence intensities within the lumen and the channel walls. While some diffusion was observed in both channels with and without an endothelial lining, corresponding with previously reported results with 70 kDa dextran tracers [12, 47], the presence of a HUVEC monolayer resulted in significantly reduced dextran diffusion after

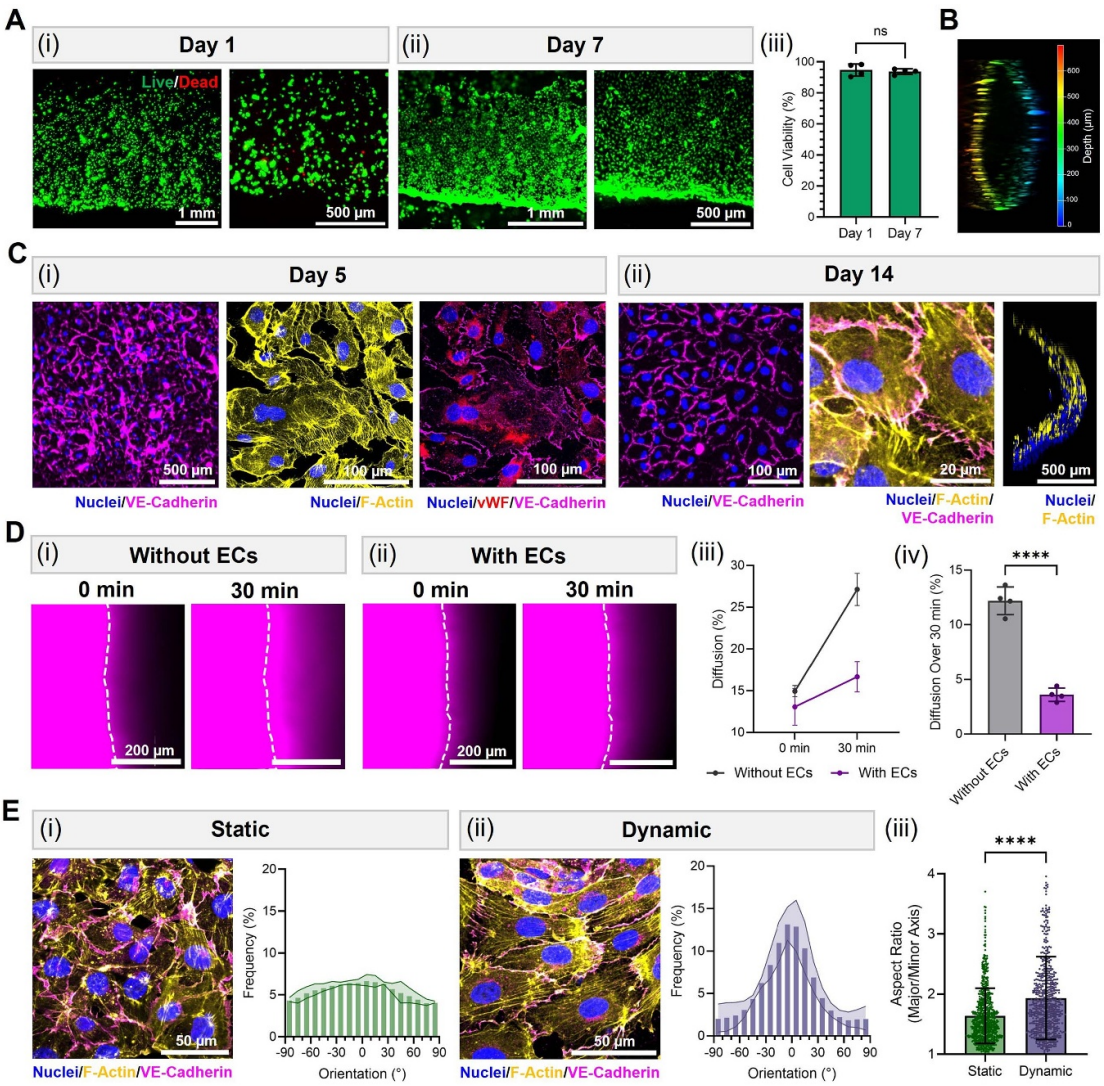

Figure 4. Sacrificial ink-based endothelialization is conducive to endothelial cell viability, proliferation, and function. (A) HUVEC seeded from the sacrificial ink maintain high viability on printed channels, as shown by representative Live/Dead images (i) 1 d and (ii) 7 d post-seeding, along with (iii) the corresponding cell viabilities ($n = 4$ replicate printed structures, unpaired t test, ns: not significant). (B) Depth-coded 3D reconstruction of HUVEC-lined channel, stained for viable cells (calcein-AM) 14 d post-seeding, shows an endothelial lining throughout the channel perimeter. (C) Sacrificial ink-seeded HUVEC exhibit stable cell–cell contacts on the print lumen, as shown by representative immunofluorescence images of VE-cadherin and F-actin after (i) 5 d and (ii) 14 d of culture. (D) Endothelial barrier function was assessed by injecting rhodamine-dextran (70 kDa) into HUVEC-lined channels after 8 d of culture. Fluorescence images were taken 0 and 30 min after perfusion of rhodamine-dextran into (i) acellular channels and (ii) HUVEC-lined channels, and diffusion into the channel walls (calculated as percentage intensity) was compared (iii) at 0 and 30 min and (iv) over the 30 min timeframe ($n = 4$ replicate printed structures, unpaired t test, $^{****}p < 0.0001$). (E) Sacrificial ink-seeded HUVEC exhibit a change in morphology under dynamic flow culture, as shown by representative immunofluorescence images and their corresponding F-actin orientation distributions (principal orientation $= 0°$; $n = 3$) under (i) static and (ii) dynamic conditions after 14 d. (iii) HUVEC lining printed channels exhibit a significantly greater aspect ratio under dynamic flow culture (data from one representative biological replicate shown, $n > 614$ cells analyzed, two-tailed Mann–Whitney test, $^{****}p < 0.0001$, $N = 2$ biological replicates).

30 min compared to acellular controls (figure 4(D), panels iii–iv). Altogether, these results indicate that the endothelial lining was able to provide vascular-mimetic barrier function.

In addition to its barrier properties, an important characteristic of a biomimetic EC lining is its response to fluid shear stress. To determine the dynamic flow response, we exposed bioprinted, sacrificial ink-seeded HUVEC channels to bidirectional flow after an initial static overnight incubation. As compared to static culture controls, flow-exposed HUVEC exhibited a more elongated morphology under dynamic culture, as well as alignment of F-actin filaments in neighboring cells (figure 4(E), panels i–ii). Quantification of cell elongation revealed a significantly higher aspect ratio for HUVEC under dynamic culture (mean = 1.93) as compared to those under static culture (mean = 1.64, $p < 0.0001$; figure 4(E), panel iii). These results demonstrate that our bioprinted channels are able to mimic the shear stress response of the native EC lining, including cell elongation and flow-induced alignment.

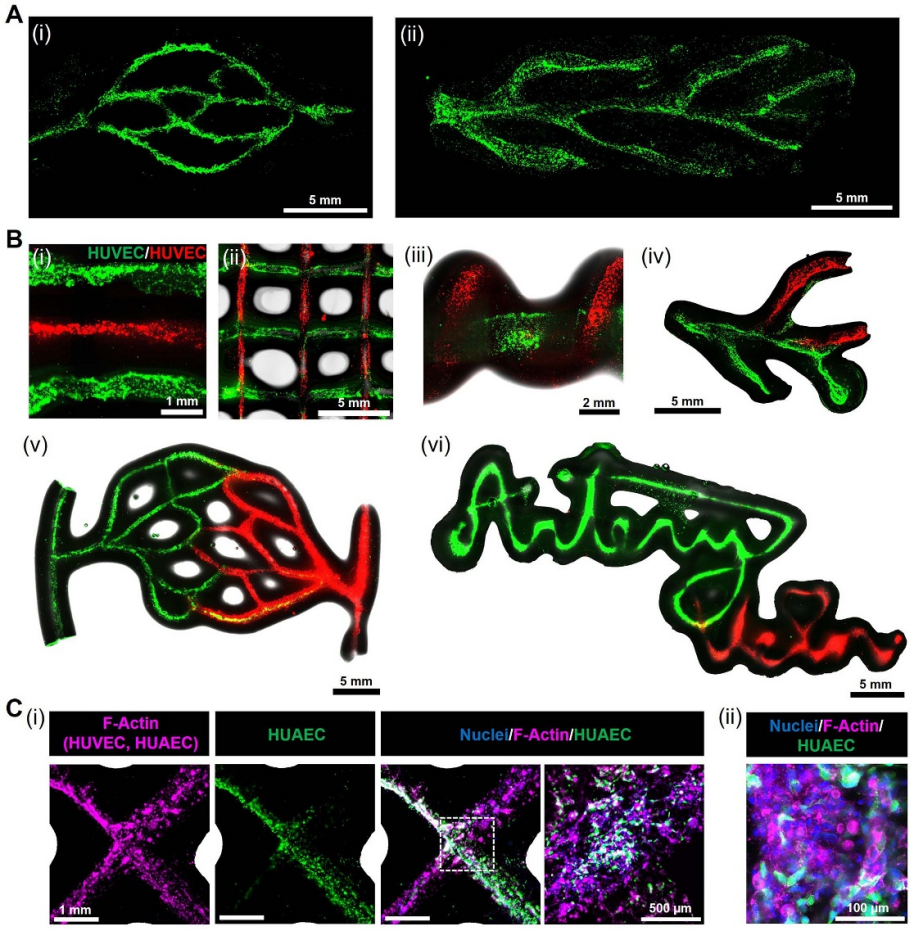

Figure 5. Sacrificial ink-based endothelialization enables the fabrication of complex, physiologically relevant networks. (A) Fluorescence images of (i) interconnected and (ii) branched vascular-like networks seeded with HUVEC from the sacrificial ink. (B) Fluorescence images of multi-cellular structures seeded with RFP-labeled HUVEC (red) and CellTracker Green-labeled HUVEC (green) from two sacrificial bioinks: (i) parallel channels; (ii) lattice; (iii) helix; (iv) branched vascular-like network; (v) interconnected vascular-like network; (vi) channels illustrating 'artery' and 'vein'. (C) Representative immunofluorescence images of arterial–venous-like structures seeded with HUVEC (unlabeled) and human umbilical artery endothelial cells (HUAEC; GFP-labeled) after 3 d of culture: (i) intersection between arterial and venous channels; (ii) magnified view of arterial and venous cells at channel junction.

2.4. Fabrication of complex, endothelialized vascular mimics through the precise patterning of sacrificial bioinks

By combining diffusion-based extrusion bioprinting with *in situ* endothelialization from the sacrificial ink, our approach enables the fabrication of complex, EC-lined networks mimicking the branched and interconnected structure of vasculature (figure 5(A)). This biofabrication strategy involves short working times due to the rapid print generation process and minimal manual manipulation required for endothelialization. For all structures demonstrated, the entire process of print generation and endothelialization was performed within 30 min, making the process highly scalable and amenable to cell viability. Furthermore, the structures presented in this study illustrate a range of channel sizes (∼0.3–2 mm inner diameter) which can be fabricated and endothelialized.

Since cells are seeded as part of the printing process, our strategy further enables the precise spatial patterning of more than one EC phenotype within a single print. Through the spatially defined extrusion of two sacrificial, cell-delivering inks, multi-cellular structures can be fabricated with branches containing different EC populations, which can be either interconnected or parallel (figure 5(B)). Furthermore, the embedded bioprinting process enables freeform 3D patterning, allowing different EC populations to be patterned into non-planar structures such as helices (figure 5(B), panel iii). This was initially demonstrated by sacrificial ink seeding of two different pre-labeled HUVEC populations.

To create more physiologically relevant structures, we then demonstrated the patterning of two different EC phenotypes to fabricate arterial and venous structures within a single bioprinted construct. One sacrificial ink contained HUVEC, while a second sacrificial ink contained human umbilical artery endothelial cells (HUAEC). Both cell types remained viable and adherent to the patterned vascular channels 3 d after printing (figure 5(C)). Furthermore, at the junction point between the arterial-like and venous-like

channels, we observed both cell types present within the monolayer, indicating that bioprinted structures are able to support the co-culture of multiple, distinct endothelial cell types. In the future, these multi-cellular networks are expected to open new opportunities for the investigation of arterial–venous signaling and its effects on endothelial cell sorting and specification.

3. Discussion

Sacrificial ink extrusion in embedded 3D bioprinting has proven capable of fabricating complex, perfusable networks with tunable diameters and branching geometries [11–13, 32, 33]. As printed structures become more complex, however, their effective endothelialization has become an increasingly prominent challenge. Here, we present a new bioprinting approach enabling the one-step fabrication and endothelialization of self-supporting vascular networks, applying a sacrificial ink to deliver both cells and crosslinkers. As compared to conventional perfusion-based seeding of pre-fabricated networks, our *in situ* endothelialization approach results in a higher cell seeding uniformity and efficiency while negating the need for separate processing steps for endothelialization. Our new technology is especially well suited for complex, self-supporting structures with branches of varying lengths, orientations, and diameters, which are challenging to uniformly endothelialize through perfusion (figure 2). Using gelatin microparticle sacrificial inks optimized for both extrusion and cell delivery (figure 3), self-supporting structures enabling endothelial monolayer formation, barrier function, and dynamic shear stress response can be fabricated (figure 4). Furthermore, our integrated strategy imparts precise spatial control over cell patterning: By directly patterning cell-delivering inks to form the printed structure, multiple endothelial cell types can be deposited in a spatially defined manner (figure 5), enabling the fabrication of multi-cellular structures mimicking the heterogeneity in EC phenotypes present in vasculature.

While several *in situ* endothelialization strategies have been explored [17–22], our approach uniquely combines *in situ* endothelialization with diffusion-induced vessel generation to form complex, cell-laden vascular networks. Previously, the feasibility of sacrificial ink-based endothelialization has been established in other bioprinting modalities, including layer-by-layer printing [17, 18] and coaxial printing [19, 20]. By applying embedded 3D printing, our approach enables unprecedented flexibility in generating complex geometries, such as non-planar helices (figure 5(B), panel iii) and vascular networks with varying-diameter branches (figure 2(A)). Furthermore, our diffusion-based approach is readily generalizable to materials with a range of crosslinking mechanisms, including photocrosslinking, small molecule crosslinking, and enzymatic crosslinking [33], by varying the crosslinker in the sacrificial ink. In the future, different vessel materials can be employed with minimal modification to ink printability and the biofabrication process. As an additional advantage, our sacrificial ink-based strategy decouples print generation from endothelialization, since cell sedimentation and attachment occur only after sacrificial ink melting. This allows independent tuning of the print dimensions, which are specified by the crosslinker diffusion time, and the cell seeding and adhesion time. In the future, the cell seeding density on the print lumen can be predicted and optimized through calculations of the luminal surface area relative to the volume of ink extruded. This would allow the cell density to be controlled in spatially defined regions by extruding multiple sacrificial bioinks with different cell densities.

Building on these demonstrations, this strategy holds promise to be applied to fabricate and endothelialize more complex 3D networks mimicking vasculature. To demonstrate the cell seeding strategy, we focused on structures with $<$5 mm height due to the fluorescence imaging depth limit for cells within the printed structure. We anticipate that the demonstrated advantages of our process over conventional perfusion-based seeding, including greater cell seeding homogeneity and efficiency, would be applicable to larger and more complex 3D structures. For larger-scale vascular networks, imaging techniques such as light-sheet microscopy may be applied to overcome imaging depth and signal attenuation limitations of conventional fluorescence microscopy [48]. For complex 3D structures containing channels in various orientations, further optimization of cell seeding uniformity across the lumen perimeter may be achieved by rotating the structure during incubation, such as using a motorized rotation device [16]. Towards the fabrication of more complex networks, systems for triggered crosslinker release could be designed to improve diffusion control during the printing process. In the current process, the crosslinker begins diffusing from the start of the print. While the structures demonstrated in this study involved relatively short print times ranging from 10 s to 2.5 min (table S1), greater control over crosslinker diffusion would be beneficial to fabricate larger and more complex structures, which require longer print times.

Based on our biofabrication strategy, the vessel dimensions, including both the inner diameter and channel wall thickness, may be further optimized. In this study, cell-lined vessels of wall thicknesses 0.8–1 mm were produced with a diffusion time of 5–10 min using a fixed photoinitiator concentration (2 mM LAP). In the future, the vessel wall thickness can be designed to match physiological arteries and veins, which have varying diameter-to-thickness

ratios [49]. While we demonstrate the bioprinting of vessels with inner diameters ∼0.3–2 mm, vessels of larger diameters mimicking physiological human arteries and veins (e.g. 1.5–5.5 mm for coronary arteries [50]) could be fabricated by extruding multiple adjacent filaments or modulating the nozzle size. On the contrary, vessels of smaller diameters can be integrated into the bioprinted structure by combining our sacrificial ink extrusion approach with microvessel generation strategies. For instance, vasculogenesis can be induced through endothelial cell loading in the surrounding matrix, and sprouting angiogenesis can be promoted through pro-angiogenic signaling [5, 51, 52]. The integration of these complementary strategies would enable the generation of capillary-scale features (e.g. $<$100 μm in diameter), which are below the typical resolution limit of extrusion-based bioprinting [53].

Importantly, our approach represents the first instance of patterning different EC populations into multi-cellular networks of physiologically relevant dimensions. The ability to create such multi-cellular models is key to recapitulating native vasculature, which consists of specialized EC populations that vary both within and between organs [39, 40]. By patterning different EC populations, such as venous and arterial cell types, within defined regions of bioprinted structures, cell–cell interactions and the effects of microenvironmental cues on cell behavior can be studied in a precisely controlled manner. For example, co-cultures of arterial and venous cells have been found to exhibit greater segregation at interfaces than co-cultures with two populations of either arterial or venous cells, a phenomenon that is controlled by Eph–ephrin signaling [41]. Looking forward, our multi-cellular, bioprinted vascular models would enable studies of arterial–venous signaling and vascular morphogenesis with more complex arterial–venous cellular configurations. Building upon our demonstration of EC alignment in response to dynamic flow, further studies may also be performed to characterize the effect of flow rate, vessel size, and shear stress level on EC behavior, for instance comparing the effects of physiological venous and arterial shear stresses on bioprinted, endothelialized channels. In addition to studying interactions between different endothelial cell types, our approach can be employed to fabricate advanced *in vitro* models of vascular disease by patterning cells with healthy and diseased phenotypes within defined regions of bioprinted networks [54]. These models may inform the development of targeted treatments that take into account the heterogeneity of endothelial cell phenotypes.

In addition to the ability to freely vary vessel diameters and branching geometries, the microstructure of printed structures can be readily tuned by varying the support bath composition. This would facilitate the encapsulation of additional cell types within the channel walls. In the future, to facilitate spreading of encapsulated cells, structures can be generated with reduced GelMA concentrations, such as 10% GelMA [33, 55]. Furthermore, porosity can be introduced into the generated channels through the incorporation of sacrificial microgels [56, 57]. Moreover, vasculogenesis may be induced by loading endothelial cells into the support bath, and sprouting angiogenesis from printed vessels may be promoted through the application of pro-angiogenic signals. Expanding beyond vascular models, our sacrificial ink-based cell seeding approach is expected to be applicable to any cell type, paving the way for other physiologically relevant bioprinted systems, such as models of airway channels, reproductive tracts, and the gastrointestinal tract. Looking forward, we envision that this approach will uncover opportunities for the fabrication of *in vitro* models of perfusable systems for disease modeling and drug screening applications along with *in vivo* regenerative medicine applications.

4. Conclusion

In summary, we have developed an integrated strategy to directly generate complex, endothelialized arterial–venous networks by combining sacrificial ink-based endothelialization with diffusion-based, embedded 3D bioprinting. Using gelatin microparticles as the carrier for both cells and crosslinkers, self-supporting, perfusable structures with varying diameters and branching geometries can be generated and uniformly endothelialized. We show that this strategy provides greater cell seeding uniformity and efficiency than conventional perfusion-based seeding, enabling the endothelialization of self-supporting networks of arbitrary branching geometries. Endothelial cells seeded onto the print lumen maintain high viability, form a stable, confluent monolayer, and exhibit vascular-mimetic barrier function and shear stress response. Importantly, our strategy enables the precise spatial patterning of different endothelial cell populations, such as arterial and venous cells, through the extrusion of multiple sacrificial, cell-delivering inks in one print. With its control over vessel dimensions and branching geometry, coupled with its ability to spatially pattern multiple endothelial cell types, this strategy enables the generation of multi-cellular vascular mimics with enhanced structural and biological complexity.

5. Materials and methods

5.1. Ink and gel precursor support bath preparation

As the base of the gel precursor support material, GelMA was synthesized using a protocol described previously [33]. Gelatin from cold water fish skin (Sigma-Aldrich) was dissolved at 20 wt% in 0.1 M

carbonate–bicarbonate buffer at 37 °C. After adjusting the pH to 10, the gelatin solution was heated to 70 °C, and methacrylic anhydride (MAA, 94%, Sigma-Aldrich) was added dropwise at 83 μl per gram of gelatin while stirring at 200 rpm. The reaction proceeded at 70 °C for 2 h. GelMA was then precipitated and collected after pouring the reaction mixture into ∼3x reaction volume of ethanol. After drying for >24 h, GelMA was dissolved in deionized water and heated to 80 °C–90 °C for at least 1 h while stirring to remove residual ethanol. The GelMA concentration (in w/v%) was determined as the percent dry mass. Gel precursor support baths were prepared by mixing stock solutions of GelMA, bovine fibrinogen (MP Biomedicals), and Aristoflex Ammonium Acryloyldimethyltaurate/VC Copolymer (AVC; Lotioncrafter) to achieve a final concentration of 20 wt% GelMA + 0.5 wt% fibrinogen + 2 wt% Aristoflex AVC.

To prepare the sacrificial ink, lyophilized gelatin microparticles (LifeSupport, FluidForm Inc.) were hydrated using cold PBS or cell culture medium. For studies of cell morphology and functionality, the pH of the gelatin microparticle slurry was adjusted to ∼7. A stock solution of lithium phenyl-2,4,6-trimethylbenzoylphosphinate (LAP, Sigma-Aldrich) photoinitiator was added to achieve a final concentration of 2 mM.

5.2. Rheological characterization

Rheological properties of the sacrificial ink and gel precursor support bath were measured using an ARG2 stress-controlled rheometer (TA Instruments) with a 40 mm-diameter parallel plate geometry at a 1.0 mm gap height. Shear stress-sweep experiments were conducted at 25 °C and 37 °C over a stress range of 0.1–1000 Pa at a frequency of 1 Hz. The viscosity of materials was measured at increasing shear rates in the range of 0.1–1000 s^{-1}. To assess self-healing, alternating high and low shear strains, which are above and below the G'/G" crossover point, respectively, were applied.

5.3. 3D bioprinting

3D printing was performed using a custom-built dual-extruder bioprinter modified from a MakerGear M2 Rev E plastic 3D printer, as previously described [8, 58, 59]. Support materials were loaded in 6-well plates or polystyrene dishes. Print paths were designed using Rhinoceros (version 5.0, Robert McNeel & Associates, Seattle, WA, USA). Drawings were segmented into points using the 'Divide' function. The resultant Cartesian coordinates were translated into G-code, with the printing parameters for each structure specified in table S1.

Human umbilical vein endothelial cells (HUVEC, PromoCell), red fluorescent protein (RFP)-expressing HUVEC (RFP-HUVEC, Angio-Proteomie), and green fluorescent protein (GFP)-expressing HUAEC (GFP-HUAEC, Angio-Proteomie) were expanded to passage 4–8 in endothelial growth media (EGM-2 BulletKit, Lonza) according to the manufacturer's instructions, and culture medium was changed every other day. For sacrificial ink-based endothelialization, cells were trypsinized, counted, and resuspended in EGM-2. The cell suspension was then added to the LAP-containing gelatin microparticle ink, resulting in a cell density of 1×10^7 per ml of ink. Structures with various geometries were printed, with print times provided in table S1. After printing is complete, diffusion of the photoinitiator was allowed to occur for an additional 5–10 min. The printed structure was then crosslinked for 5 min using a 405 nm lamp (20 W, Skouphy). After crosslinking, the resulting channel structure was removed from the uncrosslinked support bath and incubated at 37 °C and 5% CO_2 for 10 min to melt the sacrificial ink. To prevent drying, 1–2 ml of cell culture media was added on top of the sample. The sample was then flipped and incubated at 37 °C for 10 min to allow cell attachment to the opposite side of the lumen. Finally, the ends of the structure were cut to allow the melted sacrificial ink to diffuse out of the structure. For perfusion-based endothelialization, a HUVEC suspension with a cell density of 10^7 ml^{-1} was injected into the lumen of printed structures until the suspension flowed out of the opposite end. Structures were incubated for 5–10 min, then flipped and incubated for 5–10 min to allow cell adhesion to the entire lumen. After endothelialization, the cell-laden structures were incubated in EGM-2 with 5 U ml^{-1} thrombin for at least two hours before switching to fresh EGM-2. For the dynamic culture of HUVEC-lined channels, prints were affixed to the bottom of a 6-well plate with a crosslinked fibrin film after overnight incubation in EGM-2 with 5 U ml^{-1} thrombin. After replacing the media, the printed channels were then placed on a rocker (Benchmark Scientific BR2000) at ∼15 rpm frequency. Cell culture medium was changed every other day thereafter. For all samples, cell culture medium was changed every other day.

5.4. Filament surface roughness assessment

To assess ink printability and filament shape fidelity, gelatin microparticle inks containing fluorescent microparticles were extruded into a GelMA (20 wt%) + AVC (2 wt%) support bath. Printed lines and lattices were imaged using a Leica THUNDER fluorescence microscope using the 2.5X objective. Roughness profiles for the filament edges were generated via thresholding in Fiji. The average surface roughness (R_a) was then calculated as

$$R_a = \frac{|Z_1| + |Z_2| + \cdots + |Z_N|}{N} \quad (1)$$

where Z_x is the profile height at point x and N is the total number of points in the roughness profile.

5.5. Analysis of cell sedimentation

Theoretical parameters for cell motion were calculated according to equations described previously [60]. The theoretical average displacement of cells due to Brownian motion was calculated using the following equation:

$$\bar{x} = \left(\frac{RTt}{3\pi\eta r N_A}\right)^{1/2} \quad (2)$$

where R is the ideal gas constant, T is absolute temperature (25 °C for unmelted inks and 37 °C for melted inks), t is time (1800 s), η is solution viscosity, r is cell radius (measured as 7.5 μm using Countess 3 automated cell counter), and N_A is Avogadro's number.

The cell sedimentation velocity was calculated using Stokes' law as follows:

$$v = \frac{2(\rho_c - \rho)d^2 g}{9\eta} \quad (3)$$

where d is cell diameter (measured as 15 μm using Countess 3 automated cell counter), ρ_c is cell density (assumed to be 1.03 g cm^{-3} [60]), ρ is solution density (equal to 1 g cm^{-3}), g is gravitational acceleration, and η is solution viscosity.

To measure cell sedimentation within the sacrificial ink, RFP-HUVEC were encapsulated at a concentration of 10^6 ml^{-1}, and 100 μl of cell-loaded ink was cast onto each well of a 96-well plate using a positive displacement pipette. The plate was incubated at either room temperature or 37 °C in a stage-top incubator system (Tokai Hit STX) for 30 min. During incubation, Z-stack images were taken every 5 min on a Leica THUNDER fluorescence microscope using a 10X objective. Cell count in images taken at 100 μm depth intervals was quantified using Fiji (version 2.14) [61].

5.6. Endothelial permeability assay

Endothelial barrier function was assessed using a protocol similar to that reported previously [14]. A solution of 0.5 mg ml^{-1} 70 kDa rhodamine-dextran (Sigma-Aldrich) in EGM-2 was injected into printed channels with and without a HUVEC lining. Images were taken 0 and 30 min after dye injection on a Leica THUNDER fluorescence microscope using a 10X objective. The percentage diffusion (%D) of rhodamine-dextran was quantified at 0 and 30 min based on the average fluorescence intensities within the lumen and the channel walls (over a distance of ~300 μm from the lumen):

$$\%D = \frac{\text{Avg.Int. (Channel Walls)}}{\text{Avg.Int (Lumen)} + \text{Avg.Int. (Channel Walls)}}. \quad (4)$$

5.7. Cell viability assay

To assess cell viability after release from the sacrificial ink, HUVEC were encapsulated in the gelatin microparticle ink at a density of 2×10^5 ml^{-1}, and 100 μl was cast onto each well of a 48-well plate using a positive displacement pipette. The ink was incubated for 15 min at 37 °C, after which 1 ml of EGM-2 was added to each well. As a control, 100 μl of cell suspension in EGM-2 (2×10^5 ml^{-1}) was pipetted directly onto each well.

Cell viability was assessed by staining live cells with calcein-AM and dead cells with ethidium homodimer-1 (EthD-1) using a Live/Dead staining kit (Thermo Fisher Scientific). Samples were incubated in a solution of calcein-AM (2 μM) and EthD-1 (4 μM) for 30 min at 37 °C. Cells were imaged using a Leica THUNDER fluorescence microscope using 2.5X, 10X, and 20X objectives. Images were analyzed using Fiji (version 2.14) [61]. Live and dead cells were counted by thresholding and particle analysis, and cell viability was calculated as the ratio of live cells to all cells.

5.8. Estimation of cell attachment and coverage

To estimate cell attachment in sacrificial ink-seeded channels, channels of length 2 cm (i.e. extrusion volume 20 μl; table S1) were printed and endothelialized with RFP-HUVEC using the protocol described in section 5.3. A non-cell-adherent polystyrene petri dish was used to prevent attachment of leaked cells to the dish surface. After incubation of the channels for 10 min on both the top and bottom halves, the channel ends were cut open, and cell culture media was added to a total of 5 ml volume. Samples were incubated for 30 min to allow unattached cells to be released into the surrounding media. After incubation, the cell density in the surrounding medium was determined using a Countess 3 automated cell counter ($n = 6$ printed structures, with 4 measurements per sample). The total number of unattached cells was then calculated and divided by the total number of printed cells (2×10^5 cells per sample) to obtain the percentage cell leakage from sacrificial ink-seeded channels.

To evaluate cell coverage along the channel perimeter, channels seeded with RFP-HUVEC from the sacrificial ink were imaged on the top and bottom surfaces, where the bottom surface was defined as the surface seeded initially. Z-stack images (1 mm depth) were captured using a Leica THUNDER fluorescence microscope using a 2.5X objective. To quantify cell count on the top and bottom surfaces, maximum-projection images were analyzed by thresholding and particle analysis using Fiji [61].

5.9. Immunostaining and imaging of printed structures

For immunostaining, printed structures were fixed for 30 min using 4% paraformaldehyde in PBS, then washed three times with PBS for 15 min. Cells were permeabilized with 0.1% Triton X-100 in PBS (PBST) for 1 h at room temperature. Blocking was then performed with 0.05% Triton X-100, 5% normal goat serum (NGS), and 0.5 wt% bovine serum albumin

(BSA, Roche) in PBS for 3 h at room temperature. Primary antibodies VE-cadherin (rabbit mAb, Cat. #2500, Cell Signaling Technology, 1:250) and anti-vWF (mouse mAb, ab194405, Abcam, 1:250) diluted in 0.05% Triton X-100, 2.5% NGS, and 0.25 wt% BSA were applied overnight at 4 °C. Removal of unbound primary antibodies was then performed by washing samples with PBST four times for 20 min. Fluorescently tagged secondary antibodies (goat anti-rabbit, Alexa Fluor 488 or 647, Thermo Fisher Scientific; goat anti-mouse, Alexa Fluor 546, Thermo Fisher Scientific), again diluted in PBS with 0.05% Triton X-100, 2.5% NGS and 0.25% BSA, were applied for 1 h at room temperature, followed by three washes with PBST for 20 min. Cell nuclei and actin cytoskeleton were stained through incubation with 4′,6-diamidino-2-phenylindole, dihydrochloride (DAPI, Thermo Fisher Scientific, 1 μg ml^{-1}) and Alexa Fluor Plus 647 Phalloidin (Thermo Fisher Scientific) for 1 h at 37 °C, followed by three washes with PBST for 15 min. Samples were imaged using either a Leica STELLARIS 5 confocal microscope or a Leica THUNDER fluorescence microscope. For high-resolution confocal imaging, samples were additionally mounted onto coverslips with ProLong Gold Antifade reagent (Thermo Fisher Scientific). Representative images were processed using Fiji (version 2.14), and analysis of F-actin orientation distributions was performed with confocal images using the Fiji plugin OrientationJ [62].

5.10. Computational modeling of flow dynamics during perfusion seeding

Perfusion of particles through printed structures was simulated using the particle tracing module in COMSOL Multiphysics (version 6.2). The model geometry was imported with an STL file corresponding to the G-code path. For the particle release model with a Newtonian formulation and specified release times, solid particles of diameter 10 μm were released from the inlet once every 10 s for figure 1(D) and once every second for figures 2(A)–(C), with a group of 10 particles per release. A laminar, incompressible flow model was employed with initial values of 0 m s^{-1} for velocity and 0 Pa for pressure within the domain of each structure. A no slip boundary condition was applied at the channel walls. For all models, a mass flow rate of 1 ml h^{-1} was used. Representative snapshots of particle perfusion were taken at a perfusion time of 100 s for figure 1(D), 15 s for figure 2(A), and 30 s for figures 2(B) and (C).

For theoretical seeding efficiency calculations, the model endpoint was taken as the time at which all particle trajectories from the branch with higher resistance reached the outlet, representing homogeneous seeding within each branch. The number of particles present within the structure, as well as the number of particles at the outlet boundary, was counted, and the theoretical seeding efficiency was calculated as the ratio of retained to total particles.

5.11. Statistical analysis

Results were plotted in GraphPad Prism (version 10.1). Descriptions of statistical methods for each figure are included in the figure captions. Data are presented as the mean ± standard deviation unless otherwise specified.

Data availability statement

All data that support the findings of this study are included within the article (and any supplementary files).

Acknowledgment

S C H acknowledges support from the National Science Foundation (DMR 2103812 and CBET 2033302), the Advanced Research Projects Agency for Health (ARPA-H) under Award Number AY1AX000002, and the National Institutes of Health (R01 EB027171, R01 HL142718, R01 HL151997 and R01 EB027666). S S acknowledges support from the National Research Foundation of Korea (NRF) Grant funded by the Korean government (MSIT) (RS-2023-00209708). B C acknowledges support from the Stanford Knight-Hennessy Scholars program and Stanford Bio-X Bowes Fellowship. S G acknowledges support from the Novo Nordisk Foundation, Denmark, Grant No. NNF22OC0073507. J G R acknowledges support from the NSF Graduate Research Fellowship Program (GRFP) (DGE-1656518) and the Stanford Smith Family Graduate Fellowship. L G B acknowledges support from the National Science Foundation (DGE-165618), the National Institutes of Health (F31-EY034785) and the ARCS Foundation (ARCS Scholarship). R R R acknowledges support from the National Institutes of Health from the Eunice Kennedy Shriver National Institute of Child Health and Human Development (K12-HD000850) and the Stanford Maternal and Child Health Research Institute Clinical Trainee. The content is solely the responsibility of the authors and does not necessarily represent the official views of the agencies listed above.

ORCID iDs

Betty Cai https://orcid.org/0000-0002-2160-4167
David Kilian https://orcid.org/0000-0003-3151-3637
Sadegh Ghorbani https://orcid.org/0000-0002-9591-7721
Julien G Roth https://orcid.org/0000-0002-7560-3258
Alexis J Seymour https://orcid.org/0000-0002-8354-1325

Lucia G Brunel https://orcid.org/0000-0003-0327-5635
Daniel Ramos Mejia https://orcid.org/0009-0003-5374-3289
Sean Chryz Iranzo https://orcid.org/0009-0000-0439-0550
Rameshwar R Rao https://orcid.org/0000-0003-0136-2807
Sungchul Shin https://orcid.org/0000-0001-6957-6428
Sarah C Heilshorn https://orcid.org/0000-0002-9801-6304

References

[1] Mandrycky C J, Howard C C, Rayner S G, Shin Y J and Zheng Y 2021 Organ-on-a-chip systems for vascular biology *J. Mol. Cell. Cardiol.* **159** 1–13
[2] Carrabba M and Madeddu P 2018 Current strategies for the manufacture of small size tissue engineering vascular grafts *Front. Bioeng. Biotechnol.* **6** 41
[3] Gui L and Niklason L E 2014 Vascular tissue engineering: building perfusable vasculature for implantation *Curr. Opin. Chem. Eng.* **3** 68–74
[4] Fleischer S, Tavakol D N and Vunjak-Novakovic G 2020 From arteries to capillaries: approaches to engineering human vasculature *Adv. Funct. Mater.* **30** 1910811
[5] Seymour A J, Westerfield A D, Cornelius V C, Skylar-Scott M A and Heilshorn S C 2022 Bioprinted microvasculature: progressing from structure to function *Biofabrication* **14** 022002
[6] O'Connor C, Brady E, Zheng Y, Moore E and Stevens K R 2022 Engineering the multiscale complexity of vascular networks *Nat. Rev. Mater.* **7** 702–16
[7] Jia W *et al* 2016 Direct 3D bioprinting of perfusable vascular constructs using a blend bioink *Biomaterials* **106** 58–68
[8] Lee A, Hudson A R, Shiwarski D J, Tashman J W, Hinton T J, Yerneni S, Bliley J M, Campbell P G and Feinberg A W 2019 3D bioprinting of collagen to rebuild components of the human heart *Science* **365** 482–7
[9] Grigoryan B *et al* 2019 Multivascular networks and functional intravascular topologies within biocompatible hydrogels *Science* **364** 458–64
[10] Kinstlinger I S *et al* 2020 Generation of model tissues with dendritic vascular networks via sacrificial laser-sintered carbohydrate templates *Nat. Biomed. Eng.* **4** 916–32
[11] Kolesky D B, Truby R L, Gladman A S, Busbee T A, Homan K A and Lewis J A 2014 3D bioprinting of vascularized, heterogeneous cell-laden tissue constructs *Adv. Mater.* **26** 3124–30
[12] Kolesky D B, Homan K A, Skylar-Scott M A and Lewis J A 2016 Three-dimensional bioprinting of thick vascularized tissues *Proc. Natl Acad. Sci. USA* **113** 3179–84
[13] Wu W, DeConinck A and Lewis J A 2011 Omnidirectional printing of 3D microvascular networks *Adv. Mater.* **23** H178–83
[14] Ryma M *et al* 2022 A print-and-fuse strategy for sacrificial filaments enables biomimetically structured perfusable microvascular networks with functional endothelium inside 3D hydrogels *Adv. Mater.* **34** e2200653
[15] Miller J S *et al* 2012 Rapid casting of patterned vascular networks for perfusable engineered three-dimensional tissues *Nat. Mater.* **11** 768–74
[16] Kinstlinger I S, Calderon G A, Royse M K, Means A K, Grigoryan B and Miller J S 2021 Perfusion and endothelialization of engineered tissues with patterned vascular networks *Nat. Protocols* **16** 3089–113
[17] Ouyang L, Armstrong J P K, Chen Q, Lin Y and Stevens M M 2020 Void-free 3D bioprinting for *in situ* endothelialization and microfluidic perfusion *Adv. Funct. Mater.* **30** 1908349
[18] Lee V K, Kim D Y, Ngo H, Lee Y, Seo L, Yoo S-S, Vincent P A and Dai G 2014 Creating perfused functional vascular channels using 3D bio-printing technology *Biomaterials* **35** 8092–102
[19] Cui H *et al* 2019 *In vitro* and *in vivo* evaluation of 3D bioprinted small-diameter vasculature with smooth muscle and endothelium *Biofabrication* **12** 015004
[20] Gao G, Park W, Kim B S, Ahn M, Chae S, Cho W-W, Kim J, Lee J Y, Jang J and Cho D-W 2021 Construction of a novel *in vitro* atherosclerotic model from geometry-tunable artery equivalents engineered via in-bath coaxial cell printing *Adv. Funct. Mater.* **31** 2008878
[21] Zhang S, Qi C, Zhang W, Zhou H, Wu N, Yang M, Meng S, Liu Z and Kong T 2023 *In situ* endothelialization of free-form 3D network of interconnected tubular channels via interfacial coacervation by aqueous-in-aqueous embedded bioprinting *Adv. Mater.* **35** e2209263
[22] Soliman B G *et al* 2023 Programming delayed dissolution into sacrificial bioinks for dynamic temporal control of architecture within 3D-bioprinted constructs *Adv. Funct. Mater.* **33** 2210521
[23] Cai B, Kilian D, Ramos Mejia D, Rios R J, Ali A and Heilshorn S C 2023 Diffusion-based 3D bioprinting strategies *Adv. Sci.* **11** e2306470
[24] Norotte C, Marga F S, Niklason L E and Forgacs G 2009 Scaffold-free vascular tissue engineering using bioprinting *Biomaterials* **30** 5910–7
[25] Tabriz A G, Hermida M A, Leslie N R and Shu W 2015 Three-dimensional bioprinting of complex cell laden alginate hydrogel structures *Biofabrication* **7** 045012
[26] Ouyang L, Armstrong J P K, Lin Y, Wojciechowski J P, Lee-Reeves C, Hachim D, Zhou K, Burdick J A and Stevens M M 2020 Expanding and optimizing 3D bioprinting capabilities using complementary network bioinks *Sci. Adv.* **6** eabc5529
[27] Dolati F, Yu Y, Zhang Y, Jesus A M D, Sander E A and Ozbolat I T 2014 *In vitro* evaluation of carbon-nanotube-reinforced bioprintable vascular conduits *Nanotechnology* **25** 145101
[28] Gao Q, He Y, Fu J, Liu A and Ma L 2015 Coaxial nozzle-assisted 3D bioprinting with built-in microchannels for nutrients delivery *Biomaterials* **61** 203–15
[29] Wang Y, Kankala R K, Zhu K, Wang S-B, Zhang Y S and Chen A-Z 2019 Coaxial extrusion of tubular tissue constructs using a gelatin/GelMA blend bioink *ACS Biomater. Sci. Eng.* **5** 5514–24
[30] Zhou X, Nowicki M, Sun H, Hann S Y, Cui H, Esworthy T, Lee J D, Plesniak M and Zhang L G 2020 3D bioprinting-tunable small-diameter blood vessels with biomimetic biphasic cell layers *ACS Appl. Mater. Interfaces* **12** 45904–15
[31] Wang D *et al* 2022 Microfluidic bioprinting of tough hydrogel-based vascular conduits for functional blood vessels *Sci. Adv.* **8** eabq6900
[32] Skylar-Scott M A, Uzel S G M, Nam L L, Ahrens J H, Truby R L, Damaraju S and Lewis J A 2019 Biomanufacturing of organ-specific tissues with high cellular density and embedded vascular channels *Sci. Adv.* **5** eaaw2459
[33] Shin S, Brunel L G, Cai B, Kilian D, Roth J G, Seymour A J and Heilshorn S C 2023 Gelation of uniform interfacial diffusant in embedded 3D printing *Adv. Funct. Mater.* **33** 2307435
[34] Ouyang L, Burdick J A and Sun W 2018 Facile biofabrication of heterogeneous multilayer tubular hydrogels by fast diffusion-induced gelation *ACS Appl. Mater. Interfaces* **10** 12424–30
[35] Ching T, Vasudevan J, Chang S-Y, Tan H Y, Sargur Ranganath A, Lim C T, Fernandez J G, Ng J J, Toh Y-C and

Hashimoto M 2022 Biomimetic vasculatures by 3D-printed porous molds *Small* **18** 2203426
[36] Bazilevs Y, Hsu M-C, Benson D J, Sankaran S and Marsden A L 2009 Computational fluid–structure interaction: methods and application to a total cavopulmonary connection *Comput. Mech.* **45** 77–89
[37] Hynes W F, Pepona M, Robertson C, Alvarado J, Dubbin K, Triplett M, Adorno J J, Randles A and Moya M L 2020 Examining metastatic behavior within 3D bioprinted vasculature for the validation of a 3D computational flow model *Sci. Adv.* **6** eabb3308
[38] Trimm E and Red-Horse K 2023 Vascular endothelial cell development and diversity *Nat. Rev. Cardiol.* **20** 197–210
[39] Hennigs J K, Matuszcak C, Trepel M and Körbelin J 2021 Vascular endothelial cells: heterogeneity and targeting approaches *Cells* **10** 2712
[40] Krüger-Genge A, Blocki A, Franke R-P and Jung F 2019 Vascular endothelial cell biology: an update *Int J. Mol. Sci.* **20** 4411
[41] Stewen J *et al* 2024 Eph-ephrin signaling couples endothelial cell sorting and arterial specification *Nat. Commun.* **15** 2539
[42] Dejana E 1987 Fibrinogen induces adhesion, spreading, and microfilament organization of human endothelial cells *in vitro J. Cell Biol.* **104** 1403–11
[43] Shen M, Wang L, Gao Y, Feng L, Xu C, Li S, Wang X, Wu Y, Guo Y and Pei G 2022 3D bioprinting of *in situ* vascularized tissue engineered bone for repairing large segmental bone defects *Mater. Today* **16** 100382
[44] Noda K, Zhang J, Fukuhara S, Kunimoto S, Yoshimura M and Mochizuki N 2010 Vascular endothelial-cadherin stabilizes at cell–cell junctions by anchoring to circumferential actin bundles through α- and β-catenins in cyclic AMP-Epac-Rap1 signal-activated endothelial cells *Mol. Biol. Cell* **21** 584–96
[45] Millán J, Cain R J, Reglero-Real N, Bigarella C, Marcos-Ramiro B, Fernández-Martín L, Correas I and Ridley A J 2010 Adherens junctions connect stress fibres between adjacent endothelial cells *BMC Biol.* **8** 11
[46] Claesson-Welsh L, Dejana E and McDonald D M 2021 Permeability of the endothelial barrier: identifying and reconciling controversies *Trends Mol. Med.* **27** 314–31
[47] Pauty J, Usuba R, Takahashi H, Suehiro J, Fujisawa K, Yano K, Nishizawa T and Matsunaga Y T 2017 A vascular permeability assay using an *in vitro* human microvessel model mimicking the inflammatory condition *Nanotheranostics* **1** 103–13
[48] Poologasundarampillai G, Haweet A, Jayash S N, Morgan G, Moore J E and Candeo A 2021 Real-time imaging and analysis of cell-hydrogel interplay within an extrusion-bioprinting capillary *Bioprinting* **23** e00144
[49] Müller B, Lang S, Dominietto M, Rudin M, Schulz G, Deyhle H, Germann M, Pfeiffer F, David C and Weitkamp T 2008 High-resolution tomographic imaging of microvessels. *Developments in x-ray Tomography VI* vol 7078 (SPIE) pp 89–98
[50] Waller B F, Orr C M, Slack J D, Pinkerton C A, Van Tassel J and Peters T 1992 Anatomy, histology, and pathology of coronary arteries: a review relevant to new interventional and imaging techniques—part I *Clin. Cardiol.* **15** 451–7
[51] Kim S, Lee H, Chung M and Jeon N L 2013 Engineering of functional, perfusable 3D microvascular networks on a chip *Lab Chip* **13** 1489–500
[52] Wang X, Phan D T T, Sobrino A, George S C, Hughes C C W and Lee A P 2016 Engineering anastomosis between living capillary networks and endothelial cell-lined microfluidic channels *Lab Chip* **16** 282–90
[53] Traore M A and George S C 2017 Tissue engineering the vascular tree *Tissue Eng.* B **23** 505–14
[54] Ma X, Liu J, Zhu W, Tang M, Lawrence N, Yu C, Gou M and Chen S 2018 3D bioprinting of functional tissue models for personalized drug screening and *in vitro* disease modeling *Adv. Drug Deliv. Rev.* **132** 235–51
[55] Nichol J W, Koshy S T, Bae H, Hwang C M, Yamanlar S and Khademhosseini A 2010 Cell-laden microengineered gelatin methacrylate hydrogels *Biomaterials* **31** 5536–44
[56] Seymour A J, Shin S and Heilshorn S C 2021 3D printing of microgel scaffolds with tunable void fraction to promote cell infiltration *Adv. Healthcare Mater.* **10** e2100644
[57] Ouyang L, Wojciechowski J P, Tang J, Guo Y and Stevens M M 2022 Tunable microgel-templated porogel (MTP) bioink for 3D bioprinting applications *Adv. Healthcare Mater.* **11** 2200027
[58] Pusch K, Hinton T J and Feinberg A W 2018 Large volume syringe pump extruder for desktop 3D printers *HardwareX* **3** 49–61
[59] Hull S M, Lindsay C D, Brunel L G, Shiwarski D J, Tashman J W, Roth J G, Myung D, Feinberg A W and Heilshorn S C 2021 3D bioprinting using UNIversal orthogonal network (UNION) bioinks *Adv. Funct. Mater.* **31** 2007983
[60] Na K, Shin S, Lee H, Shin D, Baek J, Kwak H, Park M, Shin J and Hyun J 2018 Effect of solution viscosity on retardation of cell sedimentation in DLP 3D printing of gelatin methacrylate/silk fibroin bioink *J. Ind. Eng. Chem.* **61** 340–7
[61] Schindelin J *et al* 2012 Fiji—an open source platform for biological image analysis *Nat. Methods* **9** 676–82
[62] Fonck E, Feigl G G, Fasel J, Sage D, Unser M, Rüfenacht D A and Stergiopulos N 2009 Effect of aging on elastin functionality in human cerebral arteries *Stroke* **40** 2552–6